

ON THE COMPUTATION OF SINGULAR INTEGRALS OVER TRIANGULAR SURFACES IN \mathbb{R}^3

HRVOJE DODIG¹, MARIO CVETKOVIĆ² & DRAGAN POLJAK²

¹University of Split, Faculty of Maritime Studies, Croatia

²University of Split, Faculty of Electrical Engineering, Croatia

ABSTRACT

Various integral equation formulations and the related numerical solutions either via Boundary Element Method (BEM) or Method of Moments (MoM) require tedious calculation of double surface integrals arising from the use of vector triangular basis functions. This paper presents an accurate technique for computation of these integrals by first converting the surface integrals to contour integrals facilitating the decomposition of boundary integral to the sum of line integrals over triangle edges. It was shown that application of this technique to a Laplace type of equations yields expressions having analytical solutions. Moreover, although the same was not possible to achieve in case of integrals involving Helmholtz kernels, nonetheless, the technique enabled the computation of surface integrals to a machine accuracy by employing the adaptive quadrature rules. This approach could be found useful in the high frequency computational dosimetry.

Keywords: boundary element method, Helmholtz equation, Laplace equation, adaptive quadrature, contour integrals.

1 INTRODUCTION

Boundary element method (BEM) is a domain reduction method for solving partial differential equations (PDE's). In contrast to finite element method (FEM), BEM requires surface-only discretization. The versatility of BEM is well known, and nowadays BEM found applications in elasticity problems [1], [2], acoustics [3], [4], electromagnetism [5], [6], seismology [7], [8] and in significant number of other engineering applications [9]–[12].

There is a number of three-dimensional (3D) BEM formulations where the domain can be reduced using Green's theorems and the field $\phi(\vec{r})$ at observation point \vec{r} can be expressed as the surface integral [13]–[15]:

$$\alpha(\vec{r})\phi(\vec{r}) = \oint_{\partial V} dS' \left[G(\vec{r}, \vec{r}') \frac{\partial \phi(\vec{r}')}{\partial \vec{n}'} - \phi(\vec{r}') \frac{\partial G(\vec{r}, \vec{r}')}{\partial \vec{n}'} \right], \quad (1)$$

where ∂V is bounding surface of computational domain V , \vec{n} is an outward unit normal vector and \vec{r}' is source point. Depending on the observation point position, $\alpha(\vec{r})$ is either 0, 1/2 or 1 [16].

The Green's function $G(\vec{r}, \vec{r}')$ represents the fundamental solution to the $\mathcal{L}[G(\vec{r}, \vec{r}')] = -\delta(\vec{r}, \vec{r}')$. In case of BEM applied to Laplace or Helmholtz problem, the fundamental solution is a function of $R = |\vec{r} - \vec{r}'|$, R being the distance between the observation and the source point, respectively [17], [18].

After having discretized the boundary ∂V followed by interpolation of $\phi(\vec{r})$ and its normal derivative using shape functions N_i , the linear system of equations is obtained, containing the following two types of integrals:

$$I_1(\vec{r}) = \int_{S_\Delta} N_i(\vec{r}') G(R) dS', \quad (2)$$

$$I_2(\vec{r}) = \int_{S_\Delta} N_i(\vec{r}') \frac{\partial G(R)}{\partial \vec{n}'} dS', \quad (3)$$



where S_{Δ} is the surface of element into which the surface ∂V is discretized.

In case of regular integrals, where $\vec{r} \neq \vec{r}'$, the numerical integration of (2) and (3) is usually sufficient. For nearly singular integrals, often times it is sufficient to increase the number of integration points or the use of finer discretization is necessary. However, in case of singular integrals, where $\vec{r} = \vec{r}'$, and depending on the type of singularity, it is required to perform certain additional steps [19], such as singularity extraction [20], [21] or the so called singularity cancellation technique [22], [23], which includes transformation to polar coordinates or domain transformation, resulting in an extra computational burden if aiming to achieve accuracy.

Hence, an accurate technique for computation of these integrals to a desirable precision could be found useful. As showed in [24], accurate computation of (2) and (3) is particularly important when BEM or MoM, respectively, are utilized in the computational dosimetry of human exposure to electromagnetic field (EMF) since the resulting numerical artifacts will significantly affect the reliability of the numerical technique for this purpose. To overcome this, the singular integrals arising in these type of problems can be computed by first converting the surface integrals to contour integrals facilitating the decomposition of boundary integral to the sum of easily and quickly computed line integrals over triangle edges.

This paper is organized as follows: following the introductory part, the shape functions over the triangular elements are given in terms of the position vector and the kernel modification is given in the second section. Some details on the procedure for converting surface integrals to contour integrals are given in the following sections. Moreover, the application to a Laplace type of equations and integrals involving Helmholtz kernels is also given as well as some numerical results for the contour integration on several test examples. The final part is related to the concluding remarks and some consideration for the future work.

2 MATHEMATICAL FORMULATION

2.1 Shape functions over triangular elements

When considering BEM for the solution to the boundary value problem in 3D, the boundary surface is usually decomposed into triangular or quadrilateral elements. In case of first order triangular element, as shown in Fig. 1, the shape functions N_i can be expressed in terms of area coordinates such as [25]:

$$N_i = \frac{A_{jk}}{A}, \quad i = 1, 2, 3; j = 2, 3, 1; k = 3, 1, 2, \quad (4)$$

where A and A_{jk} are the area of first order triangular element and areas of sub-triangles, respectively, as denoted in Fig. 1.

In order to express the shape functions N_i using the position vector \vec{r}' , the sub-areas A_{jk} are expressed as:

$$A_{ij} = \frac{1}{2} \vec{n}' \cdot (\vec{r}_j - \vec{r}') \times (\vec{r}_i - \vec{r}'), \quad (5)$$

whereas the area A of triangle $\triangle 123$ can be written as:

$$A = \frac{1}{2} \vec{n}' \cdot (\vec{r}_2 - \vec{r}_1) \times (\vec{r}_3 - \vec{r}_1). \quad (6)$$

Inserting (5) and (6) into (4) the shape functions can be written as:

$$N_i(\vec{r}') = \frac{\vec{n}' \cdot (\vec{r}_j - \vec{r}') \times (\vec{r}_k - \vec{r}')}{2A}, \quad i = 1, 2, 3; j = 2, 3, 1; k = 3, 1, 2. \quad (7)$$



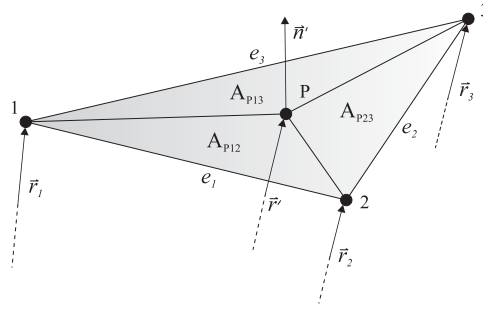


Figure 1: First order triangular element. Vectors \vec{r}_i , $i = 1, 2, 3$, are the position vectors of vertices 1, 2 and 3 whereas vector \vec{r}' is the position vector of point P . Vector \vec{n}' is the constant unit normal vector to triangle $\triangle 123$. Triangle edges are e_1 , e_2 and e_3 .

After expanding the cross product in (7), and using $\vec{r}' \times \vec{r}' = 0$, (7) can be rewritten as:

$$N_i(\vec{r}') = \frac{\vec{n}' \cdot [\vec{r}'_j \times \vec{r}'_k + \vec{r}' \times (\vec{r}'_j - \vec{r}'_k)]}{2A}, \quad i = 1, 2, 3; j = 2, 3, 1; k = 3, 1, 2. \quad (8)$$

After adding and subtracting $\vec{r}' \times (\vec{r}'_j - \vec{r}'_k)$ to the numerator of (8), where \vec{r} is the observation point Q (shown in Fig. 2), yields the following:

$$N_i(\vec{r}', \vec{r}) = \vec{n}' \cdot (\vec{r}' - \vec{r}) \times \vec{a}_i + b_i(\vec{r}), \quad (9)$$

where \vec{a}_i is a constant vector given by:

$$\vec{a}_i = \frac{\vec{r}'_j - \vec{r}'_k}{2A}, \quad (10)$$

while coefficients $b_i(\vec{r})$ are given as:

$$b_i(\vec{r}) = \frac{\vec{n}' \cdot \vec{r}'_j \times \vec{r}'_k}{2A} + \vec{n}' \cdot \vec{r} \times \vec{a}_i, \quad (11)$$

where $i = 1, 2, 3; j = 2, 3, 1; k = 3, 1, 2$.

2.2 Modification of the kernel

In order to convert the surface integrals (2) and (3) to contour integrals, the integrand first has to be appropriately transformed so the Gauss' theorem for the surface could be applied. This is done by rewriting the function $G(R)$ in the following way:

$$G(R) = \vec{n} \cdot \nabla' \times [u(R)\vec{q}], \quad (12)$$

where $R = |\vec{r} - \vec{r}'|$, ∇' is del operator acting only on primed coordinates and function $u(R)$ is given by the following integral:

$$u(R) = \int RG(R)dR. \quad (13)$$



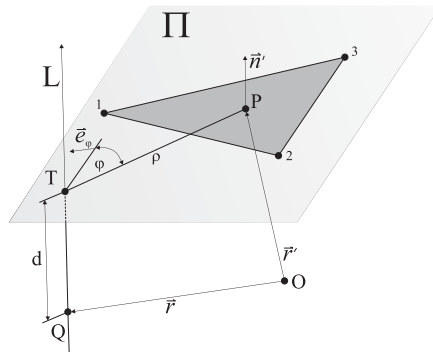


Figure 2: Triangle located in plane Π defined by unit normal vector \vec{n}' . The source and observation points are denoted by P and Q, respectively. Point T is the projection of Q on the triangle plane, while d is the distance between points Q and T.

Furthermore, vector \vec{q} can be written as:

$$\vec{q} = \frac{1}{\rho^2} \vec{n}' \times (\vec{r}' - \vec{r}), \tag{14}$$

where ρ is the distance from point T to the source point P, as shown in Fig. 2.

Applying the vector identity $\nabla \times (f\vec{A}) = \nabla f \times \vec{A} + f\nabla \times \vec{A}$, the right-hand side of (12) can be rewritten as:

$$\vec{n}' \cdot \nabla' \times [u(R)\vec{q}] = \vec{n}' \cdot \nabla' u(R) \times \vec{q} + u(R)\vec{n}' \cdot \nabla' \times \vec{q}. \tag{15}$$

The gradient $\nabla' u(R)$ can be evaluated using the chain rule as:

$$\nabla' u(R) = \sum_{i=1}^3 \frac{\partial u(R)}{\partial R} \frac{\partial R}{\partial x_i} \vec{e}_i = \frac{\partial u(R)}{\partial R} \nabla' R, \tag{16}$$

where x_i and \vec{e}_i are the coordinates and the unit ort vectors in the Cartesian coordinate system, respectively.

As the partial derivative of $u(R)$ is equal to $RG(R)$, and $\nabla' R = (\vec{r}' - \vec{r})/R$, eqn (16) thus becomes:

$$\nabla' u(R) = (\vec{r}' - \vec{r})G(R). \tag{17}$$

Inserting (14) and (17) in (15), the first term on the right hand-side term can now be rewritten as:

$$\vec{n}' \cdot \nabla' u(R) \times \vec{q} = \vec{n}' \cdot (\vec{r}' - \vec{r}) \times [\vec{n}' \times (\vec{r}' - \vec{r})] \frac{G(R)}{\rho^2}. \tag{18}$$

It is easily showed that the triple product from (18) is equal to:

$$\begin{aligned} & \vec{n}' \cdot (\vec{r}' - \vec{r}) \times [\vec{n}' \times (\vec{r}' - \vec{r})] = \\ & = \vec{n}' \cdot \vec{n}' [(\vec{r}' - \vec{r}) \cdot (\vec{r}' - \vec{r})] - [\vec{n}' \cdot (\vec{r}' - \vec{r})]^2 \\ & = R^2 - d^2 = \rho^2, \end{aligned} \tag{19}$$

where d is the distance between points Q and T , as shown on Fig. 2, thus canceling the denominator in (18):

$$\vec{n}' \cdot \nabla' u(R) \times \vec{q} = G(R). \quad (20)$$

The second term on the right-hand side of (15) is equal to zero, as vector \vec{q} can be expressed as a gradient of the cylindrical angle φ , shown on Fig. 2. As curl of any gradient vector field is equal to zero at any point except at point $\rho = 0$, this leads to $\nabla' \times \vec{q} = 0$, and thus corroborates the expression (12). However, when $\rho = 0$, the point can be excluded from the surface integrals I_1 and I_2 , as it will be shown later.

3 CONVERTING SURFACE INTEGRAL $\int N_i G dS$ TO CONTOUR INTEGRAL

To convert surface integral (2) to contour integral the shape function formulation (9) is used to write the integrand $N_i G$ as:

$$N_i(\vec{r}', \vec{r}) G(R) = \vec{n}' \cdot G(R) (\vec{r}' - \vec{r}) \times \vec{a}_i + b_i(\vec{r}) G(R). \quad (21)$$

Inserting (12) and (17) in (21), followed by some mathematical manipulation, the following is obtained:

$$N_i(\vec{r}', \vec{r}) G(R) = \vec{n}' \cdot \nabla' \times [u(R) (\vec{a}_i + b_i(\vec{r}) \vec{q})]. \quad (22)$$

After inserting (22) in (2) followed by application of Stokes' theorem yields:

$$I_1(\vec{r}) = \int_{S_\Delta} dS' \vec{n}' \cdot \nabla' \times [u(R) (\vec{a}_i + b_i(\vec{r}) \vec{q})] = \oint_{\partial S_\Delta} u(R) [\vec{a}_i + b_i(\vec{r}) \vec{q}] \cdot d\vec{l}', \quad (23)$$

where $d\vec{l}'$ is the line element along contour ∂S_Δ .

The integral (23) can be broken into sum of line integrals over triangle edges:

$$I_1(\vec{r}) = \sum_{i=1}^3 \int_{e_i} u(R) [\vec{a}_i + b_i(\vec{r}) \vec{q}] \cdot d\vec{l}' = \sum_{i=1}^3 I_1^i(\vec{r}), \quad (24)$$

where e_i are edges of the triangle shown in Fig. 1 and I_1^i is the line integral along edge e_i . Line integral I_1^i can be evaluated using:

$$I_1^i(\vec{r}) = \int_{x_1}^{x_2} u(R) \left[\vec{a} \cdot \vec{e}'_x - b_i(\vec{r}) \frac{y'}{x'^2 + y'^2} \right] dx', \quad (25)$$

where integration bounds x_1 and x_2 can be determined using $x_i = (\vec{r}_i - \vec{r}) \cdot \vec{e}'_x$, $i = 1, 2$. The derivation of (25) is omitted for brevity.

In case when point T is inside the triangle (shown on Fig. 2), we have to exclude the small area surrounding the point T and solve for the residual using some limiting process, i.e.:

$$c_i = - \lim_{\epsilon \rightarrow 0} \int_0^\alpha u(R) [\epsilon \vec{a}_i \cdot \vec{e}'_\varphi + b_i(\vec{r})] d\varphi, \quad (26)$$

where the angle α depends on the location of point T , being $\alpha = 2\pi$ (T inside the triangle), $\alpha = \pi$ (T on the edge), or a part of the circle (when T is in the vertex).



4 CONVERTING SURFACE INTEGRAL $\int N_i \frac{\partial G}{\partial \vec{n}} dS$ TO CONTOUR INTEGRAL

Integral (3) can be dealt with in a similar manner. The first step, though, is with a little effort, working out the partial derivative by taking the del operator outside the integral, i.e. (3) can be written as:

$$I_2(\vec{r}) = \int_{S_\Delta} N_i(\vec{r}') \frac{\partial G(R)}{\partial \vec{n}'} dS' = -\vec{n}' \cdot \nabla \int_{S_\Delta} N_i(\vec{r}') G(R) dS', \quad (27)$$

where $\nabla G(R) = -\nabla' G(R)$ have been used.

Inserting (23) in (27), leads to:

$$I_2(\vec{r}) = -\vec{n}' \cdot \nabla \oint_{\partial S_\Delta} u(R) [\vec{a}_i + b_i(\vec{r}) \vec{q}] \cdot d\vec{l}'. \quad (28)$$

As nabla does not act on primed coordinates, we can write $-\vec{n}' \cdot \nabla$ under the integral and then use expressions $\nabla u(R) = -\nabla' u(R)$ and $\nabla(\vec{q} \cdot d\vec{l}') = -\nabla'(\vec{q} \cdot d\vec{l}')$ to obtain:

$$\begin{aligned} I_2(\vec{r}) &= \oint_{\partial S_\Delta} [\vec{n}' \cdot \nabla' u(R)] [\vec{a}_i + b_i(\vec{r}) \vec{q}] \cdot d\vec{l}' - \oint_{\partial S_\Delta} b_i(\vec{r}) u(R) \vec{n}' \cdot \nabla(\vec{q} \cdot d\vec{l}') - \\ &\quad \oint_{\partial S_\Delta} [\vec{n}' \cdot \nabla b_i(\vec{r})] \vec{q} \cdot d\vec{l}'. \end{aligned} \quad (29)$$

It is easily showed that the last term from eqn (29) is equal to zero, since $\vec{n}' \cdot \nabla b_i(\vec{r}) = \vec{n}' \cdot \vec{a} \times \vec{n}' = 0$.

The same could be also showed for the second integral from eqn (29), although with somewhat more elaborate work. For the sake of brevity, it is suffice to say that the trick is to use the fact that vectors \vec{q} and \vec{n}' are perpendicular. So, with some clever mathematical manipulations, integrand could be rearranged so that the following could be used:

$$\vec{n}' \cdot \vec{q} = \vec{n}' \cdot \frac{1}{\rho^2} \vec{n}' \times (\vec{r}' - \vec{r}) = 0. \quad (30)$$

This means that (29) is reduced to:

$$I_2(\vec{r}) = \oint_{\partial S_\Delta} \frac{\partial u(R)}{\partial \vec{n}'} [\vec{a}_i + b_i(\vec{r}) \vec{q}] \cdot d\vec{l}', \quad (31)$$

where we have used $\frac{\partial u(R)}{\partial \vec{n}'} = \vec{n}' \cdot \nabla' u(R)$.

Integral (31) can be broken down to the sum of the easily solved line integrals over triangle edges, while in case when point T falls within the triangle, we have to perform additional computation on the residual term:

$$d_i = -\lim_{\epsilon \rightarrow 0} \int_0^\alpha \frac{\partial u(R)}{\partial \vec{n}'} [\epsilon \vec{a}_i \cdot \vec{e}\varphi + b_i(\vec{r})] d\varphi, \quad (32)$$

that, when $\rho = 0$ reduces to:

$$d_i = -b_i(\vec{r}) \frac{\partial u(|z'|)}{\partial z'} \alpha. \quad (33)$$



5 APPLICATION TO INTEGRALS INVOLVING LAPLACE KERNELS

Integrals (24) and (31) have analytical solutions for Laplace and Poisson kernels while the fundamental solution of the 3D Poisson problem is given by $G(R) = 1/4\pi R$.

If the function $u(R)$ is expressed as $u(R) = R/4\pi$, the integrand of (24) can be rewritten in the appropriate form facilitating the conversion into such contour integral having the analytical solution given as:

$$\int_{x_1}^{x_2} u(R) \vec{a}_i \cdot d\vec{l} = (\vec{a}_i \cdot \vec{e}'_x) \frac{x'R + (y'^2 + z'^2) \ln(x' + R)}{8\pi} \Bigg|_{x_1}^{x_2}, \quad (34)$$

$$\int_{x_1}^{x_2} u(R) b_i(\vec{r}') \vec{q} \cdot d\vec{l} = -b_i(\vec{r}') \frac{z' \arctan\left(\frac{x'z'}{y'R}\right) + y' \ln(x' + R)}{4\pi} \Bigg|_{x_1}^{x_2}, \quad (35)$$

where \vec{a}_i and $b_i(\vec{r}')$ are given in (10) and (11), respectively.

The integral (31), involving normal derivative of $u(R)$, can be similarly rewritten, i.e. leading to the analytical solution in the form of:

$$\int_{x_1}^{x_2} \frac{\partial u(R)}{\partial \vec{n}'} \vec{a}_i \cdot d\vec{l} = (\vec{a}_i \cdot \vec{e}'_x) \frac{z' \ln(x + R)}{4\pi} \Bigg|_{x_1}^{x_2}, \quad (36)$$

$$\int_{x_1}^{x_2} \frac{\partial u(R)}{\partial \vec{n}'} b_i(\vec{r}') \vec{q} \cdot d\vec{l} = -b_i(\vec{r}') \frac{\arctan\left(\frac{x'z'}{y'R}\right)}{4\pi} \Bigg|_{x_1}^{x_2}, \quad (37)$$

where \vec{a}_i and $b_i(\vec{r}')$ are given in (10) and (11), respectively.

6 COMPUTATION OF INTEGRALS INVOLVING HELMHOLTZ KERNELS

When the differential operator is Helmholtz operator, i.e. when function $G(R)$ satisfies:

$$\nabla^2 G(R) + k^2 G(R) = -\delta(\vec{r}, \vec{r}') \quad (38)$$

the fundamental solution is of the form:

$$G(R) = \frac{e^{-ikR}}{4\pi R}. \quad (39)$$

From (13) the function $u(R)$ can easily be computed as:

$$u(R) = \int R \frac{e^{-ikR}}{4\pi R} dR = i \frac{e^{-ikR}}{4\pi k}. \quad (40)$$

The contour integrals (24) and (31) when $u(R)$ is given by (40) do not have analytical solutions, thus, the standard Gaussian quadrature is necessary to compute the contour integrals for geometric configurations as shown in Fig. 3. However, in case when y' becomes very small, the number of Gaussian points have to be increased.

The numerical results of the contour integration for several examples as shown in Fig. 3 are given in Table 1. The results obtained using the proposed technique are compared to the numerical results obtained using the Wolfram Mathematica software.

In order to handle the singularity problem when $y' \rightarrow 0$, Gauss-Patterson adaptive quadrature [26] has been used to compute the contour integrals (24) and (31) to machine



Table 1: Comparison of contour integral results with numerical results from Wolfram Mathematica software. Number of Gauss points per triangle's edge $N = 20$.

Test case	Integral	Mathematica	Contour Integral
(a)	$\int N_1 GdS$	$0.00528364 - j0.000198499$	$0.00528364 - j0.000198499$
	$\int N_2 GdS$	$0.00528364 - j0.000198499$	$0.00528364 - j0.000198499$
	$\int N_3 GdS$	$0.00529556 - j0.0000995714$	$0.00529556 - j0.0000995714$
(b)	$\int N_1 GdS$	$0.00172243 - j0.0284663$	$0.00172243 - j0.0284663$
	$\int N_2 GdS$	$-0.00432864 + j0.0129573$	$-0.00432864 + j0.0129573$
	$\int N_3 GdS$	$0.0051389 + j0.00317481$	$0.0051389 + j0.00317481$
(c)	$\int N_1 GdS$	$0.0276113 - j0.137714$	$0.0276113 - j0.137714$
	$\int N_2 GdS$	$-0.0324167 + j0.00762088$	$-0.0324167 + j0.00762088$
	$\int N_3 GdS$	$-0.0744389 + j0.00563727$	$-0.0744389 + j0.00563727$
(d)	$\int N_1 GdS$	$0.00971219 - j0.00284063$	$0.00971219 - j0.00284063$
	$\int N_2 GdS$	$0.00797566 - j0.00559024$	$0.00797566 - j0.00559024$
	$\int N_3 GdS$	$0.00854506 - j0.00499818$	$0.00854506 - j0.00499818$
(e)	$\int N_1 GdS$	$0.00370118 - j0.00108283$	$0.00370118 - j0.00108283$
	$\int N_2 GdS$	$0.00334767 - j0.00171923$	$0.00334767 - j0.00171923$
	$\int N_3 GdS$	$0.00367605 - j0.00116374$	$0.00367605 - j0.00116374$
(f)	$\int N_1 GdS$	$-0.0138075 - j0.0103983$	$-0.0138075 - j0.0103983$
	$\int N_2 GdS$	$-0.0117517 + j0.00130501$	$-0.0117517 + j0.00130501$
	$\int N_3 GdS$	$-0.0148588 - j0.00791919$	$-0.0148588 - j0.00791919$

Table 2: The number of bisections and the number of evaluation points (EP) for adaptive Gauss-Patterson numerical integration method (AGP) as function of y' . The integral computed is $\int N_i GdS$ for Helmholtz equation using $u(R)$ given by (40).

Method	y'	Bisections	EP
AGP	1×10^{-1}	0	511
AGP	1×10^{-2}	6	604
AGP	1×10^{-4}	20	821
AGP	1×10^{-8}	52	1061
AGP	1×10^{-16}	120	2035
AGP	1×10^{-32}	260	7389

accuracy. As shown in Table 2, the drawback to this approach is the increased number of bisections when y' tends to zero. Also, in some cases one can note the decreasing numbers



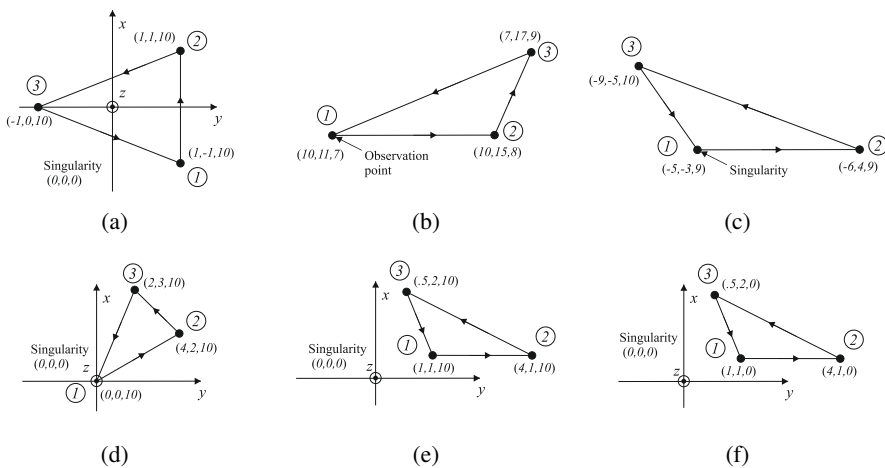


Figure 3: Several test examples for integration of $\int N_i G$ using contour integration. The integration path is denoted with arrows. Propagation constant is chosen to be $k = \frac{2\pi}{\lambda} = \frac{2\pi}{5}$. In (b) and (c) observation point is located at vertex 1.

of bisections. However, the numerical accuracy of the integration procedure converged to machine accuracy.

7 CONCLUSIONS

In this paper the technique for converting surface integrals containing Green's function and its derivative to contour integrals is shown. This conversion to contour integral is possible when Green's function is $G = G(R)$ and when indefinite integral $\int RG(R)dR$ can be computed analytically, such as in the case of Helmholtz, Laplace and Poisson type problems. It was shown that for Poisson and Laplace type of problems this technique yields analytical solutions for integrals of this type. The advantage of computation of contour integrals to surface integrals is the possibility to precisely control the accuracy of the numerical computation of these integrals when the analytical solution is not available. It has been found out that in the relatively rare cases the number of evaluation points have to be increased if the adaptive Gauss-Patterson quadrature is used. This issue is expected to be addressed in the future work within the new scheme for adaptive computation of such integrals.

REFERENCES

- [1] Simpson, R.N., Bordas, S.P.A., Trevelyan, J. & Rabczuk, T., A two-dimensional isogeometric boundary element method for elastostatic analysis. *Computer Methods in Applied Mechanics and Engineering*, **209–212**, pp. 87–100, 2012.
- [2] Elleithy, W.M., Al-Gathani, H.J. & El-Gebeily, M., Iterative coupling of BE and FE methods in elastostatics. *Engineering Analysis with Boundary Elements*, **25**, pp. 685–695, 2001.
- [3] Chen, J., Chen, K. & Chen, C.T., Adaptive boundary element method of time-harmonic exterior acoustics in two dimensions. *Computer Methods in Applied Mechanics and Engineering*, **191**, pp. 3331–3345, 2002.
- [4] Fischer, M., Gauger, U. & Gaul, L., A multipole Galerkin boundary element method for acoustics. *Engineering Analysis with Boundary Elements*, **28**, pp. 155–162, 2004.



- [5] Dodig, H., Lalléchère, S., Bonnet, P., Poljak, D. & El Khamlichi Drissi, K., Stochastic sensitivity of the electromagnetic distributions inside a human eye modeled with a 3d hybrid BEM/FEM edge element method. *Engineering Analysis with Boundary Elements*, **49**, pp. 48–62, 2014.
- [6] Dodig, H., Poljak, D. & Peratta, A., Hybrid BEM/FEM edge element computation of the thermal rise in the 3D model of the human eye induced by high frequency EM waves. *International Conference on Telecommunications and Computer Networks (SoftCOM)*, IEEE, pp. 1–5, 2012.
- [7] Kampitsis, A., Sapountzakis, E., Giannakos, S. & Gerolymos, N., Seismic soil-pile-structure kinematic and inertial interaction: A new beam approach. *Soil Dynamics and Earthquake Engineering*, **55**, pp. 211–224, 2013.
- [8] António, J. & Tadeu, A., 3D seismic response of a limited valley via BEM using 2.5D analytical Green's functions for an infinite free-rigid layer. *Soil Dynamics and Earthquake Engineering*, **22**, pp. 659–673, 2002.
- [9] Benedetti, I., Aliabadi, M.H. & Milazzo, A., A fast BEM for the analysis of damaged structures with bonded piezoelectric sensors. *Computer Methods in Applied Mechanics and Engineering*, **199**, pp. 490–501, 2010.
- [10] Chen, X. & Liu, Y., An advanced 3D boundary element method for characterizations of composite materials. *Engineering Analysis with Boundary Elements*, **29**, pp. 513–523, 2005.
- [11] Sutradhar, A. & Paulino, G.H., The simple boundary element method for transient heat conduction in functionally graded materials. *Computer Methods in Applied Mechanics and Engineering*, **193**, pp. 4511–4539, 2004.
- [12] Bush, The interaction between a crack and a particle cluster. *International Journal of Fracture*, **88**, pp. 215–232, 1997.
- [13] Brebbia, C.A. & Dominguez, J., Boundary element methods for potential problems. *Applied Mathematical Modelling*, **1**, pp. 372–378, 1977.
- [14] Cheng, A.H.-D. & Cheng, D.T., Heritage and early history of the boundary element method. *Engineering Analysis with Boundary Elements*, **29**, pp. 368–302, 2005.
- [15] Liu, Y.J., On the simple-solution method and non-singular nature of the BIE/BEM a review and some new results. *Engineering Analysis with Boundary Elements*, **29**, pp. 789–795, 2000.
- [16] Liu, Y.J. & Nishimura, N., The fast multipole boundary element method for potential problems: A tutorial. *Engineering Analysis with Boundary Elements*, **30**, pp. 371–381, 2006.
- [17] Jaswon, M.A., Integral equation methods in potential theory. I. *Proceedings of the Royal Society of London A*, **275**, pp. 23–32, 1963.
- [18] Wu, H., Liu, Y. & Jiang, W., Analytical integration of the moments in the diagonal form fast multipole boundary element method for 3-D acoustic wave problems. *Engineering Analysis with Boundary Elements*, **36**, pp. 248–254, 2012.
- [19] Cvetković, M., Poljak, D. & Drissi, K.E.K., Some computational aspects of calculation of integrals arising within the framework of method of moments-application to bioelectromagnetics. *Applied Electromagnetics and Communications (ICECOM), 2016 22nd International Conference on*, IEEE, pp. 1–6, 2016.
- [20] Khayat, M. & Wilton, D., Numerical evaluation of singular and near-singular potential integrals. *IEEE Transactions on Antennas and Propagation*, **53**(10), pp. 3180–3190, 2005.
- [21] Jarvenpaa, S., Taskinen, M. & Yla-Oijala, P., Singularity subtraction technique for high-order polynomial vector basis functions on planar triangles. *IEEE Transactions*

- on *Antennas and Propagation*, **54**(1), pp. 42–49, 2006.
- [22] Graglia, R., On the numerical integration of the linear shape functions times the 3-D Green's function or its gradient on a plane triangle. *IEEE Transactions on Antennas and Propagation*, **41**(10), pp. 1448–1455, 1993.
- [23] Li, L. & Eibert, T.F., Radial-angular singularity cancellation transformations derived by variable separation. *IEEE Transactions on Antennas and Propagation*, **64**(1), pp. 189–200, 2016.
- [24] Poljak, D., Cvetković, M., Bottauscio, O., Hirata, A., Laakso, I., Neufeld, E., Reboux, S., Warren, C., Giannopoulos, A. & Costen, F., On the use of conformal models and methods in dosimetry for nonuniform field exposure. *IEEE Transactions on Electromagnetic Compatibility*, **60**(2), pp. 328–337, 2018.
- [25] Volakis, J.L., Chatterjee, A. & Cambell, L.C., *Finite Element Method for Electromagnetics*. The IEE/OUP series on electromagnetic wave theory, IEEE Press: New York, USA, 1998.
- [26] Patterson, T.N.L., An algorithm for generating interpolatory quadrature rules of the highest degree of precision with preassigned nodes for general weight functions. *ACM Transactions on Mathematical Software*, **15**, pp. 123–136, 1989.

